The Journal of Chemical Physics

Facile synthesis of manganese (II)-doped ZnSe nanocrystals with controlled dimensionality

Cite as: J. Chem. Phys. **151**, 244701 (2019); https://doi.org/10.1063/1.5128511
Submitted: 20 September 2019 . Accepted: 03 December 2019 . Published Online: 23 December 2019

Jung Ho Yu, Junhee Kim, Taeghwan Hyeon, and Jiwoong Yang

The Journal of Chemical Physics ARTICLE scitation.org/journal/jcp

Facile synthesis of manganese (II)-doped ZnSe nanocrystals with controlled dimensionality

Cite as: J. Chem. Phys. 151, 244701 (2019); doi: 10.1063/1.5128511
Submitted: 20 September 2019 • Accepted: 3 December 2019 •
Published Online: 23 December 2019

Jung Ho Yu,[1,2,a)] Junhee Kim,[1,2,a)] Taeghwan Hyeon,[1,2,b)] and Jiwoong Yang[3,b)]

AFFILIATIONS

[1]Center for Nanoparticle Research, Institute for Basic Science (IBS), Seoul 08826, South Korea
[2]School of Chemical and Biological Engineering, Seoul National University, Seoul 08826, South Korea
[3]Department of Energy Science and Engineering, Daegu Gyeongbuk Institute of Science and Technology (DGIST), Daegu 42988, South Korea

Note: This paper is part of the JCP Special Topic on Colloidal Quantum Dots.
[a)]**Contributions:** J. H. Yu and J. Kim contributed equally to this work.
[b)]**Electronic addresses:** thyeon@snu.ac.kr and jiwoongyang@dgist.ac.kr

ABSTRACT

Doping is one of the key technologies in modern semiconductor science and industry. However, the synthetic control of doped nanocrystals is difficult to achieve. Here, we report the facile synthesis of manganese (II) doped ZnSe nanocrystals with controlled dimensionality. A strong Lewis acid-base reaction using air-stable and environmentally friendly metal chlorides as precursors can readily produce a large amount of quantum-confined ZnSe:Mn^{2+} nanocrystals. A combination of primary and secondary amines is used to control the synthetic chemistry, which enables the shape of the doped nanocrystals to be controlled. The final doping concentration of the products can be finely tunable, which is critical for carrier relaxation dynamics. It turns out that the threshold doping level for the maximum photoluminescence intensity of doped nanocrystals highly depends on their shape. Furthermore, this simple synthetic method is extendable to obtain various Mn^{2+}-doped II–VI semiconductor nanocrystals such as CdS:Mn^{2+} and ZnS:Mn^{2+}. Our study will facilitate the fundamental understanding of the doped semiconductor nanocrystals with different shapes, which is potentially useful for a wide range of applications such as lighting, photocatalysis, and bioimaging.

I. INTRODUCTION

For the past decades, semiconductor nanocrystal quantum dots (QDs) have attracted much attention due to their size- and shape-dependent properties,[1–10] and significant effort has been put into the synthesis of high-quality semiconductor nanocrystal QDs using various synthetic methods.[1,11] Doping of QDs, in combination with the quantum confinement effect, has been found to provide an effective way of tuning their optical, magnetic, and electronic properties.[4,12–14] Doped nanocrystals have become promising candidates for use in spintronics,[15,16] display/lighting,[17,18] electronics,[19–21] and biological imaging applications.[22–24] Although a lot of work has gone into the doping of semiconductor nanocrystals,[25–33] the synthesis of high-quality, doped nanocrystals remains a challenge as incorporating impurity ions into host nanocrystals is intrinsically difficult.[34,35] In general, doping of colloidal nanocrystals is known to be achieved by the adsorption of impurity ions onto the nanocrystal surface during the growth phase.[12,36–40] Consequently, doping becomes more difficult for quantum-confined nanocrystals, which prevents fundamental studies and practical applications of doped QDs.

For the shape-controlled synthesis of doped nanocrystals, the situation becomes even more complicated than the synthesis of typical spherical doped nanocrystals. Despite the recent progress in nanocrystal doping, previous studies of doped semiconductor nanocrystals have usually focused on zero-dimensional (0D) spherical nanocrystals.[12–14,17–25] The anisotropic growth of nanocrystals is usually achieved by limiting the growth of specific facets,[41] which can prohibit the dopant adsorption onto the nanocrystal surface. In addition, the anisotropic crystal morphology of many

one-dimensional (1D) or two-dimensional (2D) nanostructured materials also makes doping difficult.[36,42] Consequently, the successful doping of semiconductor nanocrystals with controlled dimensionality has rarely been reported[4,43] and usually requires nonconventional strategies. For example, 1D CdSe nanorods can be doped by diffusion doping.[44] 2D CdSe quantum wells (QWs) can be doped by atomic layer deposition doping[45,46] or nucleating-controlled doping.[4,47] These kinds of additional experimental approaches are quite complicated and limit the large-scale production of high-quality, doped nanocrystals, which is an important prerequisite for practical applications of doped nanocrystals. Overall, it is highly demanding to design a synthetic route of high-quality, doped nanocrystals with controlled dimensionality in a one-pot reaction.

Here, we report the shape-controlled synthesis of quantum-confined ZnSe:Mn^{2+} nanocrystals. A simple heat-up method using a strong Lewis acid-base reaction has been developed to selectively synthesize 0D and 1D ZnSe:Mn^{2+} nanocrystals. The shape of these doped semiconductor nanocrystals can be easily controlled by using different amines as coordinating ligands. In addition, the final doping concentration of the nanocrystals is easily modified by adjusting the ratio of the metal chloride precursors, which enables us to study its effects on the carrier relaxation dynamics of these doped nanocrystals. It is found that there exists the threshold doping concentration of maximum photoluminescence (PL) intensity and this value for 1D nanorods is smaller than that of 0D QDs. Furthermore, various Mn^{2+}-doped II–VI semiconductor nanocrystals, including CdS:Mn^{2+} and ZnS:Mn^{2+}, can be effectively produced by slightly modifying our method, which suggests its potential applicability for the general synthesis of doped nanocrystals. Our single-step synthetic method is so simple and effective that it can be easily applied in the gram-scale synthesis of doped semiconductor nanocrystals and opens new opportunities to study novel doped nanoscale semiconductors for both fundamental scientific studies and practical applications.

II. EXPERIMENTAL SECTION

A. Materials

Zinc chloride ($ZnCl_2$, 99.999%), manganese (II) chloride ($MnCl_2$, 99.999%), selenium (99.999%), elemental sulfur powder (S, 99.0%), 1-octadecene (technical grade, 90%), cadmium chloride ($CdCl_2$, 99.999%), oleylamine (97%, primary amine-value), dibenzylamine (98%), trioctylphosphine (TOP, 90%), ethyl alcohol (99.5%, anhydrous), and chloroform (99%, anhydrous) were purchased from Aldrich Chemical Co. CO gas (CO, 99.995%) was purchased from Sumitomo Seika Chemicals Co.

B. Synthesis of ZnSe:Mn^{2+} 0D QDs

All synthesis procedures were carried out under an argon atmosphere using standard Schlenk techniques. Typically for the synthesis of 3 nm-sized ZnSe:Mn^{2+} QDs, 0.5 mmol of $ZnCl_2$ and 0.14 mmol of $MnCl_2$ in 18.0 ml of dibenzylamine were heated to 150 °C under vacuum for 2 h to form metal halide–ammine complexes. Meanwhile, an oleylammonium selenocarbamate solution (0.9M) was prepared by bubbling CO gas through 10 ml of oleylamine containing 9 mmol of Se powder for 3 h at 110 °C.[48,49] Then, 4.0 ml of the oleylammonium selenocarbamate solution was injected into the metal halide–ammine complex solution at 30 °C. The mixture was heated to 260 °C, at which temperature it was maintained for 5 min. The final products were separated by standard centrifugation using 20.0 ml of ethanol and 1.0 ml of TOP, which can remove the excess selenium precursors. To control the Mn^{2+} doping concentration in the final products, the amount of the $MnCl_2$ precursor was adjusted.

For the large-scale synthesis, 7.5 mmol of $ZnCl_2$ and 2.1 mmol of $MnCl_2$ in 270.0 ml of dibenzylamine were heated to 150 °C under vacuum for 2 h. This solution was cooled to 30 °C, and then 60.0 ml of the oleylammonium selenocarbamate solution (0.9M) was injected. The temperature of the mixture was increased to 260 °C and maintained for 5 min.

To investigate the effect of the reactivity of selenium precursors for the doping of ZnSe nanocrystals, various selenium sources were tested for the synthesis. For the control experiments, TOP-Se and H_2Se were used instead of selenocarbamate, while the other experimental conditions were kept the same.

C. Synthesis of ZnSe:Mn^{2+} 1D nanorods

For the typical synthesis of ZnSe:Mn^{2+} nanorods, a mixture of 0.5 mmol of $ZnCl_2$, 0.14 mmol of $MnCl_2$, 5.0 ml oleylamine, and 5.0 ml of 1-octadecene was heated to 150 °C under vacuum for 2 h to form metal halide–ammine complexes. Meanwhile, the selenium precursor solution (oleylammonium selenocarbamate) was prepared by bubbling CO gas through oleylamine containing Se powder for 3 h at 110 °C. Then, 5.0 ml of the oleylammonium selenocarbamate solution (0.6M) was injected into the metal halide–ammine complex solution at 30 °C. This mixture was heated to 230 °C and kept at this temperature for 18 h. To control the Mn^{2+} doping concentration in the final products, the amount of $MnCl_2$ was varied.

D. Synthesis of ZnSe:Mn^{2+}/ZnS and ZnSe:Mn^{2+}/ZnSe core/shell 0D QDs

For the synthesis of Mn^{2+} doped core/shell 0D QDs, outer shells were grown onto ZnSe:Mn^{2+} 0D QDs. First, ZnSe:Mn^{2+} 0D core QDs were synthesized by the method described in the earlier part. During the synthesis of ZnSe:Mn^{2+} 0D core QDs described above, Zn and S stock solutions were prepared for the shell growth. A Zn stock solution was prepared by dissolving 1.5 mmol of $ZnCl_2$ in 6.0 ml of dibenzylamine and heating the solution to 120 °C under vacuum for 1 h to form metal halide–ammine complexes. A sulfur (S) stock solution was prepared by dissolving 4.0 mmol of elemental sulfur in 10.0 ml of dibenzylamine and heating the solution to 40 °C to form sulfur–amine complexes. ZnS shells (i.e., ZnSe:Mn^{2+}/ZnS core/shell structures) were grown by adding 2.0 ml of the Zn stock solution to the solution of the as-prepared ZnSe:Mn^{2+} 0D QDs [~0.5 mmol (based on the amount of Zn) in a mixture of amine solution containing 18.0 ml of dibenzylamine and 4.0 ml of oleylamine] at 150 °C and heating for 5 min. Then, 3.0 ml of the S stock solution was injected. This solution was heated to 260 °C and kept at this temperature for 10 min.

For the growth of ZnSe shells (i.e., ZnSe:Mn^{2+}/ZnSe core/shell structures), 2.0 ml of the Zn stock solution was added in the mixture

of the reaction solution for Mn^{2+}/ZnSe synthesis without purification. The excess amount of the Se precursor (selenocarbamate) introduced for the synthesis of core materials is used to supply Zn ions for the formation of ZnSe shells. This solution was heated to 260 °C and kept at this temperature for 10 min.

E. Synthesis of ZnS:Mn^{2+} and CdS:Mn^{2+} nanocrystals

All synthesis procedures were carried out under an argon atmosphere using standard Schlenk techniques. Typically for the synthesis of 5 nm-sized ZnS:Mn^{2+} QDs, a solution of 0.5 mmol of $ZnCl_2$, 0.02 mmol of $MnCl_2$, and 6.5 ml of dibenzylamine was heated to 150 °C under vacuum for 2 h to form metal halide–ammine complexes. Meanwhile, 3.0 mmol of elemental sulfur powder in 2.5 ml of dibenzylamine was heated to 50 °C. Then, 2.5 ml of this sulfur solution was injected into the metal halide–ammine complex solution at 30 °C. The temperature of the mixture was increased to 260 °C and maintained for 15 min. The final products were separated by standard centrifugation using 20.0 ml of ethanol.

Typically for the synthesis of CdS:Mn^{2+} 1D nanorods, 1.8 mmol of $CdCl_2$ and 0.0072 mmol of $MnCl_2$ in 12.0 ml of oleylamine were heated to 150 °C under vacuum for 2 h to form metal halide–ammine complexes. Meanwhile, 3.6 mmol of elemental sulfur powder in 6.0 ml of oleylamine was heated to 150 °C, and then, the sulfur solution was injected into the metal halide-ammine complex solution at 30 °C. The temperature of the mixture was increased to 80 °C and maintained for 24 h. The final products were separated by standard centrifugation using 20.0 ml of ethanol.

F. Characterization of Mn^{2+} doped nanocrystals

Absorption spectra were obtained with a Cary 5000E spectrometer (Agilent Technologies). Photoluminescence (PL) emission spectra were recorded with an FLS980 spectrometer (Edinburgh Instruments) equipped with a 450 W xenon lamp bulb as the light source. The PL quantum yield (QY) of the doped nanocrystals was measured using an absolute PL QY measurement system (FLS980 spectrometer equipped with an F-M01 integrating sphere). The excitation wavelength was 350 nm for the PL QY measurement for all the samples. Transmission electron microscopy (TEM) was conducted with a JEM-2100F microscope (JEOL) using a 200 kV accelerating voltage. X-ray diffraction (XRD) patterns were obtained using JP/D/MAX-2500H. The final doping concentration (x_{Mn}) of the QDs, which was calculated as the number of Mn^{2+} ions in a nanocrystal ensemble divided by the total number of Mn^{2+} and Zn^{2+} ions in the nanocrystal ensemble, was characterized by inductively coupled plasma-mass spectrometry (ICP-MS) using a NexION 350D instrument (Pekin-Elmer SCIEX) with argon plasma (6000 K). The electron paramagnetic resonance (EPR) spectra were obtained using Bruker EMX 300 at 77 K and at the microwave frequency of 9.5 GHz with 0.01 kHz resolution.

Time-resolved PL lifetime (TRPL) spectra were measured for the $^4T_1$-$^6A_1$ internal transition of the Mn^{2+} ions. Pulsed excitation light (350 nm) was generated using a μF2 pulsed xenon flash lamp (100 W), and the emitted photons were detected by a red photomultiplier tube (Red-PMT) detector. The pulsed width and repetition rate were 2–4 ms and 50 Hz, respectively.

III. RESULTS AND DISCUSSION

We have developed a new synthetic method for producing ZnSe:Mn^{2+} nanocrystals using a Lewis acid–base reaction between metal halide–ammine complexes and oleylammonium selenocarbamate (see Sec. II and Scheme 1 for experimental details). For the synthesis of ZnSe:Mn^{2+} 0D QDs, a mixture of oleylamine and dibenzylamine was used as a coordinating solvent. The crystal structure of the as-synthesized QDs was characterized by XRD and high-resolution TEM (HR-TEM). The XRD pattern of the ZnSe:Mn^{2+} 0D QDs in Fig. S1(a) shows that the positions of the diffraction peaks clearly match with the zinc blende crystal phase of ZnSe (PDF No.: 65-9602). Figures 1(a) and 1(b) show the TEM images of the ZnSe:Mn^{2+} 0D QDs. An average size of the QDs is approximately 2.9 (±0.3) nm, and their size distribution is uniform [Fig. S1(b)]. A representative HR-TEM image of a ZnSe:Mn^{2+} 0D QD shows the lattice spacing of 0.32 nm [Fig. 1(c)], which is assigned to the (111) plane of the zinc blende ZnSe crystals [Fig. 1(d)] (PDF No.: 65-9602). The final doping concentration (x_{Mn}) of the QDs is 1.24%, as determined by ICP-MS (Table S1).

ZnSe:Mn^{2+} 0D QDs were further characterized by optical spectroscopy. The absorption and photoluminescence (PL) spectra are shown in Fig. 2(a). The absorption spectrum exhibits a clear band edge transition at around 390 nm, which is blue shifted from the bulk bandgap (~480 nm) due to the quantum confinement effect.[50] The well-resolved absorption transition confirms the narrow size distribution of the synthesized nanocrystals. A clear emission in the PL spectrum at approximately 580 nm is corresponding to the $^4T_1$-$^6A_1$ internal transition of the Mn^{2+} ions,[51,52] which indicates that the Mn^{2+} ions are well incorporated into the tetrahedral cation sites of the ZnSe nanocrystal host.[53,54] The PL QY of the Mn^{2+} $^4T_1$-$^6A_1$ internal transition of these QDs is measured to be about 5%, which is a reasonable value considering the absence of the shells.

Room temperature PL lifetime measurements were carried out for the $^4T_1$-$^6A_1$ internal transition of ZnSe:Mn^{2+} 0D QDs to understand the carrier relaxation dynamics [Fig. 2(b)]. The measured carrier lifetime (τ_{avg}) of the ZnSe:Mn^{2+} 0D QDs is approximately 0.616 ms, which is comparable to conventional ZnSe:Mn^{2+} QDs.[55] Furthermore, the hyperfine splitting constant was determined to be 65.6×10^{-4} cm^{-1} based on the EPR spectrum [Fig. S2(a)], which confirms that the majority of Mn^{2+} ions are successfully incorporated into the ZnSe nanocrystal lattice.[56,57] Because the proposed synthetic procedure is simple and uses environmentally benign and air-stable metal halide precursors, it can be readily applied in

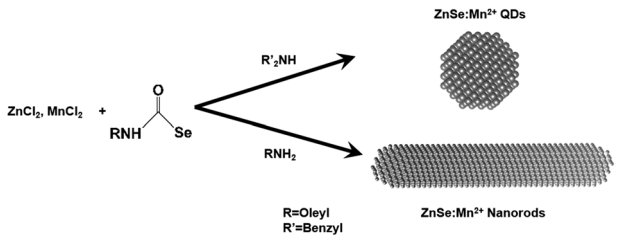

SCHEME 1. Schematic illustration of the synthesis process of 0D QDs and 1D nanorods.

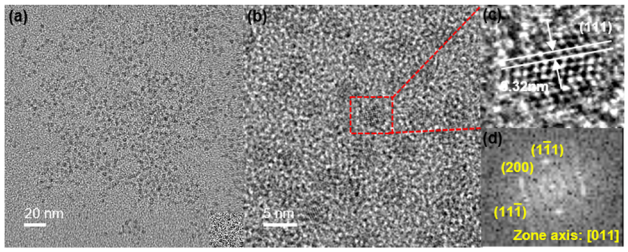

FIG. 1. (a) Low-magnification TEM image and (b) HR-TEM image of ZnSe:Mn^{2+} 0D QDs. (c) Magnified TEM image and (d) fast Fourier transform (FFT) image of the red boxed area in panel (b).

large-scale synthesis [Fig. S2(b)]. In addition, we can also synthesize ZnS:Mn^{2+} (Fig. S3) and CdS:Mn^{2+} nanocrystals (Fig. S4) by the modification of our synthesis procedures for the ZnSe:Mn^{2+} nanocrystals.

Our method using selenocarbamate can easily produce ZnSe:Mn^{2+} 0D QDs. To understand the importance of the selenium precursor for doping of ZnSe nanocrystals, we tested and compared the use of two additional selenium sources, H_2Se and TOP-Se, which are generally used as selenium precursors in the conventional nanocrystal synthesis.[58–61] When H_2Se and TOP-Se were used as the selenium precursors, the host ZnSe nanocrystals were not effectively doped with Mn^{2+} ions, as indicated by the fact that the $^4T_1$-$^6A_1$ internal transition of the Mn^{2+} ions was not observed in their PL emission spectra (Fig. S5). These results demonstrate that the selection of a selenium precursor is critical for the doping of ZnSe nanocrystals.[62]

Interestingly, the shape of nanocrystals can be systematically controlled by changing the coordinating surfactants. When oleylamine was used as a single coordinating solvent instead of the mixture of dibenzylamine and oleylamine, 1D ZnSe:Mn^{2+} nanorods were produced (Scheme 1, Fig. 3). In general, secondary amines are more basic than primary amines as the electron density of the nitrogen atom is higher in the secondary amines. Consequently, dibenzylamine forms stronger bonds with the zinc ions on the nanocrystal surface compared to oleylamine. In addition, the compact dibenzylamine has lower steric hinderance than oleylamine. Thus, it can be suggested that the surface capping density of surfactants increases when dibenzylamine is used as the coordinating ligand, which suppresses the growth of nanocrystals, resulting

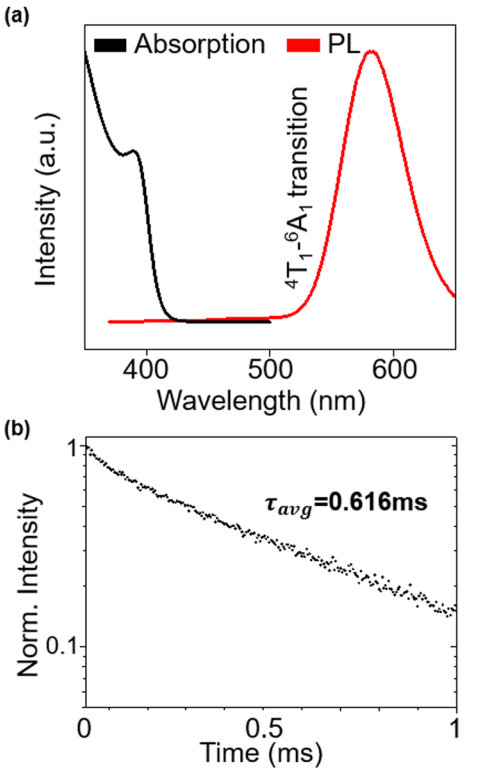

FIG. 2. (a) Absorption and PL spectra of ZnSe:Mn^{2+} QDs and (b) normalized TRPL spectra of the $^4T_1$-$^6A_1$ internal transition under 350 nm excitation.

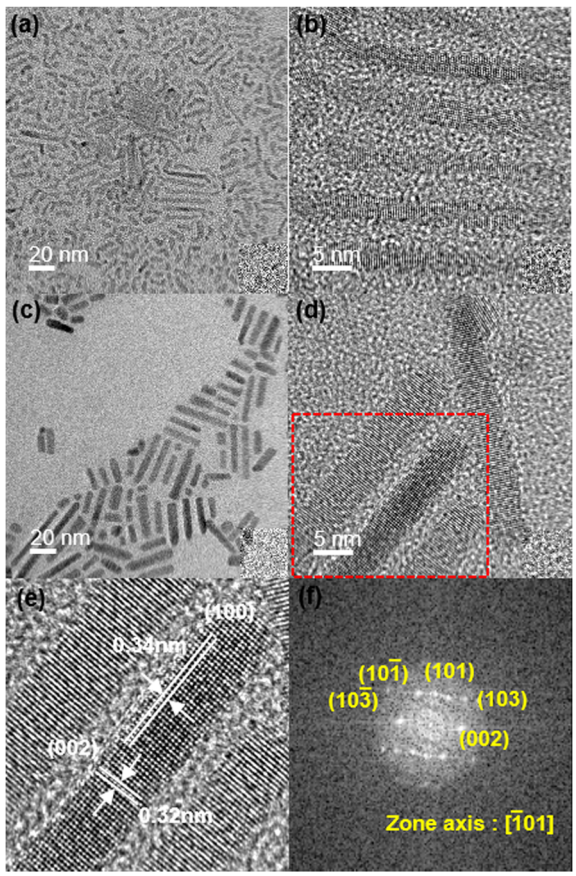

FIG. 3. (a) Low-resolution TEM image and (b) HR-TEM image of ZnSe:Mn^{2+} nanorods with a growth time of 1 h. (c) Low-resolution TEM image and (d) HR-TEM image of ZnSe:Mn^{2+} nanorods with a growth of 18 h. (e) Magnified TEM image and (f) FFT image of a ZnSe:Mn^{2+} nanorod.

in the formation of 0D spherical nanocrystals.[1,63] In addition, an anisotropic crystal structure might also be helpful for 1D growth. The crystal structure of the nanorods was characterized by XRD and HR-TEM, and the results are shown in Fig. S6 and Fig. 3, respectively. The XRD peaks of the nanorods match those of the wurtzite ZnSe crystal phase (PDF No.: 15-0105). Furthermore, the sharp peak associated with the (002) plane of the wurtzite ZnSe crystal phase indicates that these nanorods have an anisotropic shape elongated along the [002] direction. The HR-TEM image of a ZnSe:Mn^{2+} 1D nanorod shows the lattice spacing of 0.32 nm and 0.34 nm, which are assigned to the (002) and (100) planes of the wurtzite ZnSe crystals, respectively [Figs. 3(e) and 3(f)] (PDF No.: 15-0105).

We trace the growth of the nanorods as the reaction proceeds. At the initial reaction stage, the product is a mixture of 0D QDs and 1D nanorods. The crystal phase of this mixture is composed of both zinc blende and wurtzite structures. As the reaction proceeds, the proportion of 1D nanorods increases [Figs. 3(a) and 3(c)], which suggests the 1D growth of nanocrystals. The TEM image of ZnSe:Mn^{2+} 1D nanorods shows that the product is a mixture of 0D QDs and 1D nanorods [Fig. S7(a)]. Interestingly, it is found that the crystal phase of 0D QDs and 1D nanorods can be assigned to zinc blende [Figs. S7(b) and S7(c)] and wurtzite [Figs. S7(d) and S7(e)], respectively. In addition, the diameter of the ZnSe:Mn^{2+} nanorods increases with the prolonged growth time. The increase in the average diameter of nanorods (from 2.4 nm to 5.2 nm) with growth time is also shown in the TEM images [Figs. 3(b) and 3(d)] and histograms (Fig. S8). As the reaction time increases, the band edge transitions in the absorption spectra are red shifted slightly [Fig. 4(a)], which is consistent with the TEM observation. These results suggest that the diameter of ZnSe:Mn^{2+} nanorods can easily be controlled by changing the reaction time. Importantly, the relative PL intensity of the 1D nanorods varies with the growth time; when the growth time increases from 5 min to 1 h, the PL intensity of the 1D nanorods also increases. It can be attributed to the curing of the nanocrystal defects (e.g., surface defects and chlorine defects) as the particle growth. Because such defects induce deep-level energy traps, the removal of the defects strongly contributes to the increase in the PL intensity. However, as the nanorods continue to grow, the PL intensity decreases [Fig. 4(b)]. This result is consistent with the previous observation on the Mn^{2+} doped ZnS QDs, which shows that the PL intensity decreases as the size increases.[64] In contrast to the growth time-dependent change in the PL intensity, the decay time of the 1D nanorods remains almost constant [Fig. 4(c), Table S2].

We can effectively control the final doping concentration (x_{Mn}) of the ZnSe:Mn^{2+} 0D QDs by varying the amount of the manganese (Mn^{2+}) precursor. When the initial concentration of the Mn^{2+} precursor ($MnCl_2$) is increased from 22 mol. % to 40 mol. %, the final doping concentration of the 0D QDs gradually changes from 1.24% to 5.88% (Table S1). While the final doping concentration changes, the shape and energy position of the transitions observed in the absorption and PL emission spectra are nearly the same [Figs. 5(a) and 5(b)]. This suggests that the size and shape of the host nanocrystals remain the same regardless of the change in the Mn^{2+} doping concentration, which can also be confirmed by size distribution histograms acquired by TEM analysis (Fig. S9). The influence of the Mn^{2+} doping concentration on the properties of QDs can

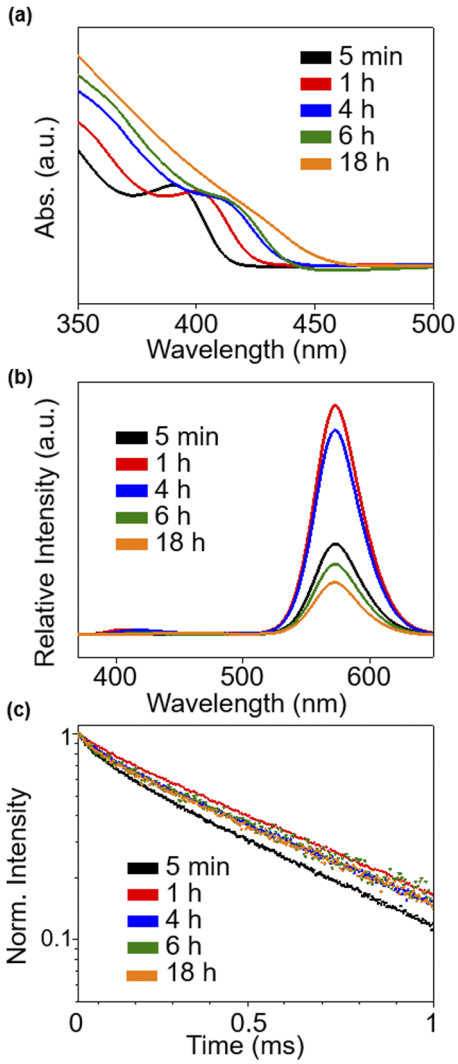

FIG. 4. (a) Absorption spectra, (b) PL spectra, and (c) normalized TRPL spectra of ZnSe:Mn^{2+} nanorods depending on the growth time.

be observed in the PL emission spectra. The PL emission peak at 395 nm, which corresponds to the ZnSe band edge transition, is clearly shown at a low doping concentration (x_{Mn} = 1.24%), while this transition almost disappears at the high doping concentration (x_{Mn} = 5.88%). This implies that a sufficient amount of Mn^{2+} is required to achieve doping of most of individual nanocrystals in the ensemble.

When the final Mn^{2+} concentration increases from 1.24% to 4.32%, the PL intensity of Mn^{2+} $^4T_1$-$^6A_1$ internal transition increases because the proportion of doped nanocrystals, which contribute to the emission at 580 nm, increases. However, a further increase in the Mn^{2+} doping concentration (x_{Mn}: from 4.32% to 5.88%) causes the PL intensity of the ZnSe:Mn^{2+} 0D QDs to decrease.

The doping concentration of the nanocrystals significantly affects the relaxation dynamics of the carriers as shown in the TRPL

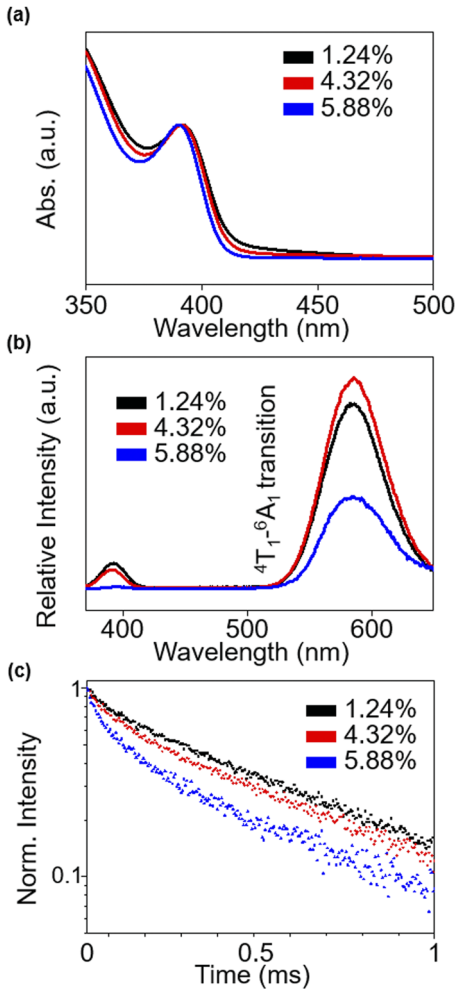

FIG. 5. (a) Absorption spectra, (b) PL spectra, and (c) normalized TRPL spectra of ZnSe:Mn^{2+} 0D QDs with various final doping concentrations.

spectra [Fig. 5(c)]. Biexponential PL decay curves were analyzed using the following equation:[65]

$$\tau_{avg} = \frac{A_1\tau_1^2 + A_2\tau_2^2}{A_1\tau_1 + A_2\tau_2}. \quad (1)$$

In this equation, A_1 and τ_1 are the normalized amplitude and the PL decay time of the recombination process of single Mn^{2+} ions, and A_2 and τ_2 are the normalized amplitude and the PL decay time of the recombination process of Mn^{2+} ion pairs.

In the ZnSe:Mn^{2+} nanocrystal system, the Mn^{2+} ions, incorporated into the lattice of ZnSe nanocrystals, exist either as single Mn^{2+} ions or as Mn^{2+} ion pairs.[66] Partly because of the spin-forbidden nature and parity of the $^4T_1$-$^6A_1$ internal transition of isolated Mn^{2+} ions and partly because of the electric dipole transition and the relaxed spin selection rule of Mn^{2+} pairs, the PL decay lifetimes of the Mn^{2+} pairs are shorter than those of the isolated Mn^{2+} ions.[67,68] In the case of the nanocrystals with a low Mn^{2+} doping concentration, the contribution of single Mn^{2+} ions is high, which means a higher A_1/A_2 ratio compared to that of nanocrystals with a high Mn^{2+} doping concentration (Table S3). Because τ_2 is shorter than τ_1, τ_{avg} of nanocrystals with a low doping concentration is longer than that of the nanocrystals with a high doping concentration. Furthermore, an increase in the number of Mn^{2+} ion pairs induces energy transfer between neighboring Mn^{2+} ions,[57] which can explain why the luminescence intensity of highly doped QDs decreases.

We can also control the final doping concentration of the 1D ZnSe:Mn^{2+} nanorods by varying the amount of the Mn^{2+} precursor (Table S4). When the initial Mn^{2+} concentration increases from 1.7 mol. % to 22 mol. %, the final doping concentration of the 1D nanorods changes from 0.23% to 3.62%. The shape and energy position of the peaks in the absorption and PL spectra remain mostly constant (Fig. 6). The effect of Mn^{2+} doping concentration on the properties of nanorods is shown in the PL emission intensity. As the final doping concentration increases (x_{Mn}: from 0.23% to 1.16%), the PL intensity of the Mn^{2+} $^4T_1$-$^6A_1$ internal transition increases because the number of Mn^{2+} ions in the ZnSe nanocrystal lattice increases. The resulting PL QY of the nanorods with the final doping concentration of 1.16% is about 2%, which is high considering the large size of these nanorods. A further increase in the doping concentration leads to the decrease in the PL intensity of the 1D ZnSe:Mn^{2+} nanorods, which is consistent with the trend observed for the 0D ZnSe:Mn^{2+} QDs.[57] Notably, the threshold doping level to maximize the PL intensity of 1D nanorods is much lower than that

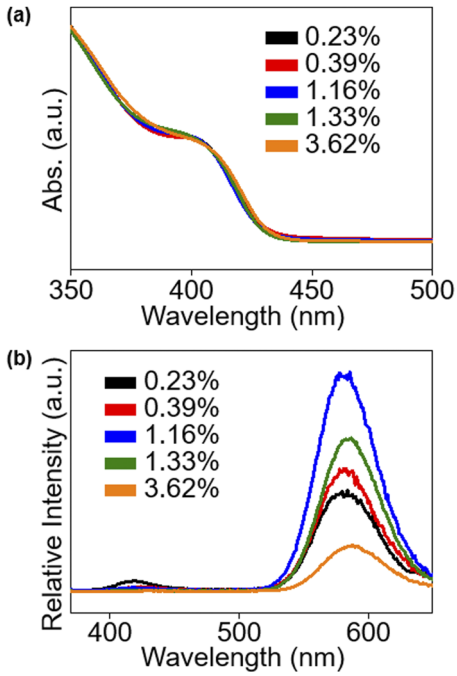

FIG. 6. (a) Absorption spectra and (b) PL spectra of ZnSe:Mn^{2+} 1D nanorods with different final doping concentrations. The growth time is fixed to 1 h for these samples.

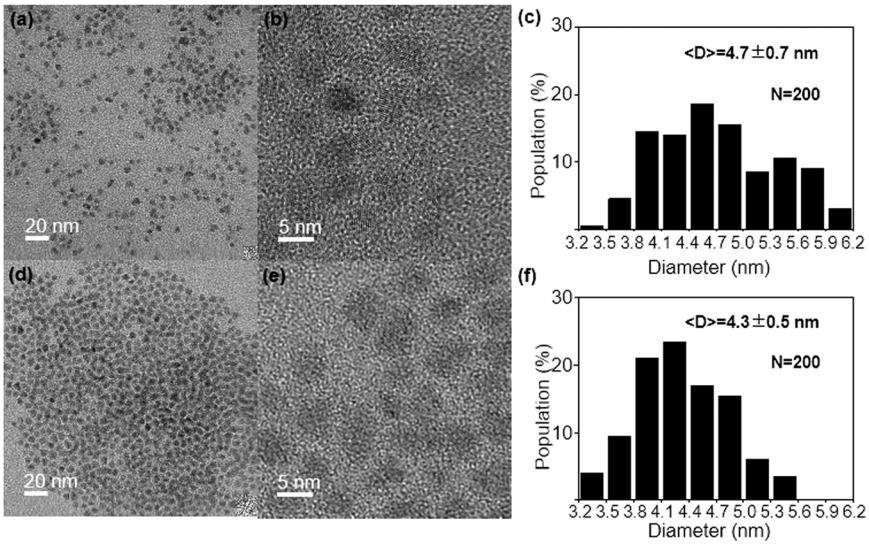

FIG. 7. (a) Low-magnification, (b) HR-TEM image, and (c) size distribution histogram of ZnSe:Mn^{2+}/ZnSe 0D QDs. (d) Low-magnification, (e) HR-TEM image, and (f) size distribution histogram of ZnSe:Mn^{2+}/ZnS 0D QDs.

of the 0D QDs (about 1% vs about 4%). This can be attributed to the fact that the proportion of undoped nanorods is much lower than that of the QDs with a similar final doping concentration because the nanorods are much larger in size than QDs.

We can improve the luminescence intensity of these ZnSe:Mn^{2+} nanocrystals by encapsulating them with ZnS or ZnSe shells[69,70] (see Sec. II for details). Figures 7(a) and 7(b) show the TEM images of ZnSe:Mn^{2+}/ZnSe core/shell QDs. The size of ZnSe:Mn^{2+}/ZnSe core/shell nanocrystals increases from 2.9 nm (±0.3 nm) to 4.7 nm (±0.7 nm) as shown in the histogram [Fig. 7(c)]. The increase in the nanocrystal diameter suggests that the ZnSe:Mn^{2+} cores are successfully encapsulated in ZnSe shells. The absorption spectra [Fig. 8(a)] show a slight red-shift of the band edge transition from 392 nm to 407 nm due to the increase in the effective radius of the host materials. As a result of the successful encapsulation, the relative PL intensity of ZnSe:Mn^{2+}/ZnSe core/shell nanocrystals is three times higher than that of the ZnSe:Mn^{2+} nanocrystals without shells [Fig. 8(c)]. This method can also be applied to obtain 1D core/shell nanocrystals showing enhanced PL intensity (Fig. S10).

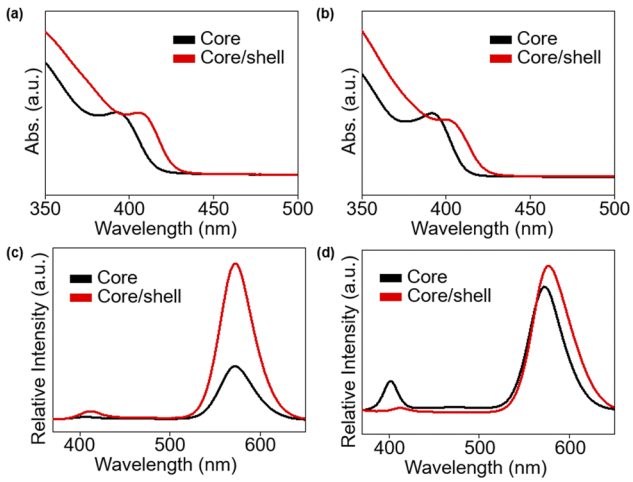

FIG. 8. Absorption spectra of (a) ZnSe:Mn^{2+} and ZnSe:Mn^{2+}/ZnSe 0D QDs and (b) ZnSe:Mn^{2+} and ZnSe:Mn^{2+}/ZnS 0D QDs. PL spectra of (c) ZnSe:Mn^{2+} and ZnSe:Mn^{2+}/ZnSe 0D QDs and (d) ZnSe:Mn^{2+} and ZnSe:Mn^{2+}/ZnS 0D QDs.

Similarly, the ZnSe:Mn^{2+} nanocrystals can be encapsulated within ZnS shells. Figures 7(d) and 7(e) display the TEM images of the ZnSe:Mn^{2+}/ZnS core/shell QDs, and the core-shell structure was also verified by line-scan energy dispersive X-ray spectroscopy (EDS, Fig. S11). The average size of the ZnSe:Mn^{2+}/ZnS core/shell nanocrystals increases from 2.9 nm (±0.3 nm) to 4.3 nm (±0.5 nm) as shown in Fig. 7(f). The red-shift in the band edge transition and the increase in the PL intensity observed for the ZnSe:Mn^{2+}/ZnSe QDs are also observed for the ZnSe:Mn^{2+}/ZnS QDs [Figs. 8(b) and 8(d)]. However, the position of the $^4T_1$-$^6A_1$ internal transition is red-shifted from 575 nm to 581 nm between the ZnSe:Mn^{2+}/ZnS QDs PL spectrum and the ZnSe:Mn^{2+}/ZnSe PL spectrum. Because of the lattice mismatch between ZnSe and ZnS (4.6%),[71] the lattice spacing of ZnSe:Mn^{2+} is compressed at the core–shell interface and the derived strain suppresses the Mn–Se bonds in the ZnSe:Mn^{2+} cores. Consequently, the crystal field splitting of the internal $^4T_1$-$^6A_1$ transition becomes smaller, which leads to its red shift in the PL spectrum.[72,73] XRD peaks are shifted toward higher angles when ZnSe nanocrystals are passivated with the ZnS shell, supporting the compressive lattice strain at the core-shell interface[74] (Fig. S12).

IV. CONCLUSION

In summary, we have synthesized quantum-confined ZnSe:Mn^{2+} nanocrystals via a facile heating-up method using a strong Lewis acid–base reaction. The dimensionality of the nanocrystals can be controlled by changing the coordinating ligands, while maintaining the successful incorporation of Mn^{2+} dopant ions into the host

nanocrystals. The proposed synthetic route is simple and readily applied to large-scale synthesis. In addition, we can finely tune the final doping concentration and systematically studied the effects on the optical properties of the doped nanocrystals. It should be noted that the doping concentration of the maximum luminescence intensity highly depends on the shape of doped nanocrystals: about 1% and 4% for 1D and 0D nanocrystals, respectively. The PL intensity of the doped nanocrystals can be further enhanced by passivating them with ZnS or ZnSe outer shells, which is important for their practical use. We envision that these shape-controlled ZnSe:Mn^{2+} nanocrystals will be applied in various applications such as lighting, photocatalysis, and bioimaging.

SUPPLEMENTARY MATERIAL

See the supplementary material for XRD patterns, TEM size distributions, and final doping concentrations.

ACKNOWLEDGMENTS

T.H. acknowledges the financial support by the Institute for Basic Science of Korea (Grant No. IBS-R006-D1). J.Y. acknowledges the financial support by the DGIST Start-up Fund Program of the Ministry of Science, ICT and Future Planning (Grant No. 2019070014).

REFERENCES

[1]C. B. Murray, D. J. Norris, and M. G. Bawendi, J. Am. Chem. Soc. **115**, 8706 (1993).
[2]D. V. Talapin, J. S. Lee, M. V. Kovalenko, and E. V. Shevchenko, Chem. Rev. **110**, 389 (2010).
[3]X. Peng, L. Manna, W. Yang, J. Wickham, E. Scher, A. Kadavanich, and A. P. Alivisatos, Nature **404**, 59 (2000).
[4]J. H. Yu, X. Liu, K. E. Kweon, J. Joo, J. Park, K. T. Ko, D. W. Lee, S. Shen, K. Tivakomsasithorn, J. S. Son, J. H. Park, Y. W. Kim, G. S. Hwang, M. Dobrowolska, J. K. Furdyna, and T. Hyeon, Nat. Mater. **9**, 47 (2010).
[5]A. I. Hochbaum and P. Yang, Chem. Rev. **110**, 527 (2010).
[6]M. R. Bergren, P. K. B. Palomaki, N. R. Neale, T. E. Furtak, and M. C. Beard, ACS Nano **10**, 2316 (2016).
[7]I. Moreels, K. Lambert, D. Smeets, D. D. Muynck, T. Nollet, J. C. Martins, F. Vanhaecke, A. Vantomme, C. Delerue, G. Allan, and Z. Hens, ACS Nano **3**, 3023 (2009).
[8]K. E. Knowles, M. T. Frederick, D. B. Tice, A. J. Morris-Cohen, and E. A. Weiss, J. Phys. Chem. Lett. **3**, 18 (2012).
[9]E. A. Weiss, R. C. Chiechi, S. M. Geyer, V. J. Porter, D. C. Bell, M. G. Bawendi, and G. M. Whitesides, J. Am. Chem. Soc. **130**, 74 (2008).
[10]A. Agrawal, I. Kriegel, and D. J. Milliron, J. Phys. Chem. C **119**, 6227 (2015).
[11]D. V. Talapin, A. L. Rogach, A. Kornowski, M. Haase, and H. Weller, Nano Lett. **1**, 207 (2001).
[12]D. J. Norris, A. L. Efros, and S. C. Erwin, Science **319**, 1776 (2008).
[13]M. Shim and P. Guyot-Sionnest, Nature **407**, 981 (2000).
[14]J. Lee, J. Yang, S. G. Kwon, and T. Hyeon, Nat. Rev. Mater. **1**, 16034 (2016).
[15]I. Zutic, J. Fabian, and S. D. Sarma, Rev. Mod. Phys. **76**, 323 (2004).
[16]F. Muckel, C. J. Barrows, A. Graf, A. Schmitz, C. S. Erickson, D. R. Gamelin, and G. Bacher, Nano Lett. **17**, 4768 (2017).
[17]A. K. Rath, S. Bhaumik, and A. J. Pal, Appl. Phys. Lett. **97**, 113502 (2010).
[18]V. Wood, J. E. Halpert, M. J. Panzer, M. G. Bawendi, and V. Bulovic, Nano Lett. **9**, 2367 (2009).
[19]C. R. Kagan, E. Lifshitz, E. H. Sargent, and D. V. Talapin, Science **353**, aac5523 (2016).
[20]J. Yang, M. K. Choi, D.-H. Kim, and T. Hyeon, Adv. Mater. **28**, 1176 (2016).
[21]D. V. Talapin and C. B. Murray, Science **310**, 86 (2005).
[22]E. S. Levy, C. A. Tajon, T. S. Bischof, J. Iafrati, A. Fernandez-Bravo, D. J. Garfield, M. Chamanzar, M. M. Maharbiz, V. S. Sohal, P. J. Schuck, B. E. Cohen, and E. M. Chan, ACS Nano **10**, 8423 (2016).
[23]O. Chen, L. Riedemann, F. Etoc, H. Herrmann, M. Coppey, M. Barch, C. T. Farrar, J. Zhao, O. T. Bruns, H. Wei, P. Guo, J. Cui, R. Jensen, Y. Chen, D. K. Harris, J. M. Cordero, Z. Wang, A. Jasanoff, D. Fukumura, R. Reimer, M. Dahan, R. K. Jain, and M. G. Bawendi, Nat. Commun. **5**, 5093 (2014).
[24]J. H. Yu, S.-H. Kwon, Z. Petrasek, O. K. Park, S. W. Jun, K. Shin, M. Choi, Y. I. Park, K. Park, H. B. Na, N. Lee, D. W. Lee, J. H. Kim, P. Schwille, and T. Hyeon, Nat. Mater. **12**, 359 (2013).
[25]D. Mocatta, G. Cohen, J. Schattner, O. Millo, E. Rabani, and U. Banin, Science **332**, 77 (2011).
[26]A. Sahu, M. S. Kang, A. Kompch, C. Notthoff, A. W. Wills, D. Deng, M. Winterer, C. D. Frisbie, and D. J. Norris, Nano Lett. **12**, 2587 (2012).
[27]N. Grumbach, A. Rubin-Brusilovski, G. I. Maikov, E. Tilchin, and E. Lifshitz, J. Phys. Chem. C **117**, 21021 (2013).
[28]P. Chakraborty, Y. Jin, C. J. Barrows, S. T. Dunham, and D. R. Gamelin, J. Am. Chem. Soc. **138**, 12885 (2016).
[29]N. Pradhan, S. D. Adhikari, A. Nag, and D. D. Sarma, Angew. Chem., Int. Ed. **56**, 7038 (2017).
[30]J. Yang, F. Muckel, W. Baek, R. Fainblat, H. Chang, G. Bacher, and T. Hyeon, J. Am. Chem. Soc. **139**, 6761 (2017).
[31]D. M. Kroupa, B. K. Hughes, E. M. Miller, D. T. Moore, N. C. Anderson, B. D. Chernomordik, A. J. Nozik, and M. C. Beard, J. Am. Chem. Soc. **139**, 10382 (2017).
[32]P. Lommens, F. Loncke, P. F. Smet, F. Callens, D. Poelman, H. Vrielinck, and Z. Hens, Chem. Mater. **19**, 5576 (2007).
[33]D. V. Talapin, C. T. Black, C. R. Kagan, E. V. Shevchenko, A. Afzali, and C. B. Murray, J. Phys. Chem. C **111**, 13244 (2007).
[34]D. A. Schwartz, N. S. Norberg, Q. P. Nguyen, J. M. Parker, and D. R. Gamelin, J. Am. Chem. Soc. **125**, 13205 (2003).
[35]Y. Yang, O. Chen, A. Angerhofer, and Y. C. Cao, J. Am. Chem. Soc. **130**, 15649 (2008).
[36]S. C. Erwin, L. Zu, M. I. Hafel, A. L. Efros, T. A. Knnedy, and D. J. Norris, Nature **436**, 91 (2005).
[37]J. D. Bryan and D. R. Gamelin, Prog. Inorg. Chem. **54**, 47 (2005).
[38]M.-H. Du, S. C. Erwin, and A. L. Efros, Nano Lett. **8**, 2878 (2008).
[39]B. B. Srivastava, S. Jana, and N. Pradhan, J. Am. Chem. Soc. **133**, 1007 (2011).
[40]R. Buonsanti and D. J. Milliron, Chem. Mater. **25**, 1305 (2013).
[41]Z. A. Peng and X. Peng, J. Am. Chem. Soc. **123**, 1389 (2001).
[42]Y. Yin and A. P. Alivisatos, Nature **437**, 664 (2005).
[43]P. T. K. Chin, J. W. Stouwdam, and R. A. J. Janssen, Nano Lett. **9**, 745 (2009).
[44]V. A. Vlaskin, C. J. Barrows, C. S. Erickson, and D. R. Gamelin, J. Am. Chem. Soc. **135**, 14380 (2013).
[45]S. Delikanli, M. Z. Akgul, J. R. Murphy, B. Barman, Y. Tsai, T. Scrace, P. Zhang, B. Bozok, P. L. Hernadez-Martinez, J. Christodoulides, A. N. Cartwright, A. Petrou, and H. V. Demir, ACS Nano **9**, 12473 (2015).
[46]F. Muckel, S. Delikanli, P. L. Hernadez-Martinez, T. Priesner, S. Lorenz, J. Ackermann, M. Sharma, H. V. Demir, and G. Bacher, Nano Lett. **18**, 2047 (2018).
[47]M. Sharma, K. Gungor, A. Yeltik, M. Olutas, B. Guzelturk, Y. Kelestemur, T. Erdem, S. Delikanli, J. R. McBride, and H. V. Demir, Adv. Mater. **29**, 1700821 (2017).
[48]N. Sonoda, T. Yasuhara, K. Kondo, T. Ikeda, and S. Tsutsumi, J. Am. Chem. Soc. **93**, 6344 (1971).
[49]J. Yang, R. Fainblat, S. G. Kwon, F. Muckel, J. H. Yu, H. Terlinden, B. H. Kim, D. lavarone, M. K. Choi, I. Y. Kim, I. Park, H.-K. Hong, J. Lee, J. S. Son, Z. Lee, K. Kang, S.-J. Hwang, G. Bacher, and T. Hyeon, J. Am. Chem. Soc. **137**, 12776 (2015).
[50]A. P. Alivisatos, Science **271**, 933 (1996).
[51]R. N. Bhargava, D. Gallagher, X. Hong, and A. Nurmikko, Phys. Rev. Lett. **72**, 416 (1994).

[52]N. Pradhan and X. Peng, J. Am. Chem. Soc. **129**, 3339 (2007).
[53]Y. Yang, O. Chen, A. Angerhofer, and Y. C. Cao, J. Am. Chem. Soc. **128**, 12428 (2006).
[54]S. Acharya, D. D. Sarma, N. R. Jana, and N. Pradhan, J. Phys. Chem. Lett. **1**, 485 (2009).
[55]C. Gan, Y. Zhang, D. Battaglia, X. Peng, and M. Xiao, Appl. Phys. Lett. **92**, 241111 (2008).
[56]D. J. Norris, N. Yao, F. T. Charnock, and T. A. Kennedy, Nano Lett. **1**, 3 (2001).
[57]V. K. Sharma, S. Gokyar, Y. Kelestemur, T. Erdem, E. Unal, and H. V. Demir, Small **10**, 4961 (2014).
[58]M. K. Choi, J. Yang, D. C. Kim, Z. Dai, J. Kim, H. Seung, V. S. Kale, S. J. Sung, C. R. Park, N. Lu, T. Hyeon, and D.-H. Kim, Adv. Mater. **30**, 1703279 (2018).
[59]M. K. Choi, J. Yang, K. Kang, D. C. Kim, C. Choi, C. Park, S. J. Kim, S. I. Chae, T. H. Kim, T. Hyeon, and D.-H. Kim, Nat. Commun. **6**, 7149 (2015).
[60]M. Marudachalam, H. Hichri, R. Klenk, R. W. Birkmire, and W. N. Shafarman, Appl. Phys. Lett. **67**, 3978 (1995).
[61]H. Liang, U. Avachat, W. Liu, J. V. Duren, and M. Le, Solid-State Electron. **76**, 95 (2012).
[62]L. Lian, Y. Xia, C. Zhang, B. Xu, L. Yang, H. Liu, D. Zhang, K. Wang, J. Gao, and J. Zhang, Chem. Mater. **30**, 982 (2018).
[63]J. J. Christensen, R. M. Izatt, D. P. Wrathall, and L. D. Hansen, J. Chem. Soc. A **89**, 1212 (1969).
[64]H. Wang and H. Li, Chalcogenide Lett. **8**, 309 (2011).
[65]H. Chauhan, Y. Kumar, and S. Deka, Nanoscale **6**, 10347 (2014).
[66]S. Acharya, S. Sarkar, and N. Pradhan, J. Phys. Chem. C **117**, 6006 (2013).
[67]W. Park, T. C. Jones, W. Tong, S. Schon, M. Chaichimansour, B. K. Wagner, and C. J. Summers, J. Appl. Phys. **84**, 6852 (1998).
[68]A. Ishizumi, E. Jojima, A. Yamamoto, and Y. Kanemitsu, J. Phys. Soc. Jpn. **77**, 053705 (2008).
[69]W. K. Bae and J. Lim, Korean J. Chem. Eng. **36**, 173 (2019).
[70]D. Lee, S. Koh, D. Yoon, S. Lee, W. D. Kim, D. Kim, W. K. Bae, J. Lim, and D. C. Lee, Korean J. Chem. Eng. **36**, 1518 (2019).
[71]C.-S. Hwang and I.-H. Cho, Bull. Korean Chem. Soc. **26**, 1776 (2005).
[72]A. M. Smith, A. M. Mohs, and S. Nie, Nat. Nanotechnol. **4**, 56 (2009).
[73]G. H. Li, F. H. Su, B. S. Ma, K. Ding, S. J. Xu, and W. Chen, Phys. Status Solidi B **241**, 3248 (2004).
[74]S. Mangel, L. Houben, and M. B. Sadan, Nanoscale **8**, 17568 (2016).